Thirteenth USA/Europe Air Traffic Management Research and Development Seminar (ATM2019)

Condensation Trails in Trajectory Optimization

Judith Rosenow and Hartmut Fricke
Technische Universität Dresden
Institute of Logistics and Aviation
Dresden, Germany
Email: Judith.Rosenow@tu-dresden.de

***Abstract*—Contrails are one of the driving contributors on global warming, induced by aviation. The impact of contrails on global warming is subject to large uncertainties of more than $100\,\%$. In detail, condensation trails might even change the algebraic sign between a cooling and a warming effect in an order of magnitude, which is comparable to the impact of aviation emitted Carbon dioxides and Nitrogen oxides. This implies the necessity to granularly consider the environmental impact of condensation trails in single trajectory optimization tools. The intent of this study is the elaboration of all significant factors deciding on the net effect of single condensation trails. Possible simplifications will be proposed for a consideration in single trajectory optimization tools. Finally, the effects of the most important impact factors, such as latitude, time of the year and time of the day, wind shear, atmospheric turbulence and their consideration in a multi-criteria trajectory optimization tool are exemplified. The results can be used for an arbitrary trajectory optimization tool with environmental optimization intents.**

Keywords: Contrails, Trajectory Optimization, Energy efficiency, Weather impact

I. Introduction

Condensation trails (contrails) summarize a type of human induced clouds, developed behind aircraft due to condensation of exhausted water vapor emissions and ambient humidity around exhausted soot particles and atmospheric condensation nuclei [1] in a cold ambient atmosphere, satisfying the Schmidt-Appleman-criterion [2, 3]. In an ice supersaturated environment, those artificial ice clouds form into long living cirrus clouds called "Cirrus homogenitus" as defined by the World Meteorological Organization [4].

In the Earth-atmosphere energy budget, contrails act like a barrier [5–7]. They scatter incoming shortwave solar radiation back to the sky (resulting in a cooling effect) and they absorb and emit the outgoing longwave terrestrial radiation back to the Earth's surface (yielding a warming effect in the lower layer of the atmosphere) [6, 8–10]. The dominating effect may be defined as radiative forcing RF, as the imbalance in the radiation budget of the Earth-atmosphere system (considering the instantaneous response of the stratosphere). The contribution of contrails to global warming is a subject to uncertainties and depends on flight performance, weather conditions and time. Latest combinations of several approaches to model a global impact of contrails on global warming summarize a warming net effect of $RF_{\mathrm{Contrail}} = 0.05\ \mathrm{W\,m^{-2}}$ with uncertainties between -0.02 and $+0.15\ \mathrm{W\,m^{-2}}$ for 2010 [6]. Single studies result in a larger environmental impact of contrails including negative (cooling) net effects (e.g. $RF_{\mathrm{Contrail}} = -0.007$ to $+\,0.02\ \mathrm{W\,m^{-2}}$ for 2005 [9]). Compared to the summed effect of one year's aviation emitted Carbon dioxide CO_2 and Nitrogen oxides NO_x which is $RF_{CO_2,NO_x} = 0.04\ \mathrm{W\,m^{-2}}$ [6], the impact of contrails on global warming is no longer negligible [6, 11], because it might exceed those effects of CO_2 and NO_x, although contrails are only formed during $10\,\%$ of the flight, on a global average [12]. Thus, the need for contrails to be considered in trajectory optimization becomes indisputable.

The impact of single condensation trails on trajectory optimization has been analyzed by Gounou et al. [13] and Forster et al. [14] focusing on the importance of large solar zenith angles during sunset and sunrise. In an application of a Monte Carlo code for photon transport, Forster et al. [14] already considered effects like multiple scattering, but in a coarse spatial grid and ignoring the impact of flight performance on the optical properties of the contrail. Detailed studies on all significant impact factors have been elaborated by Rosenow [11]. In the current study, the results have been simplified and harnessed for trajectory optimization. All other research interests known to the authors concentrated on the effect of contrails on a global scale. Using global climate models and historic air traffic data, reliable estimations of the global contrail radiative forcing for the year 2000 of $RF_{\mathrm{Contrail}} = 0.03\ (-0.01\ \text{to} + 0.08)\ \mathrm{W\,m^{-2}}$ [9] have been improved for 2010 to $RF_{\mathrm{Contrail}} = 0.02\ (-0.01\ \text{to} + 0.03)\ \mathrm{W\,m^{-2}}$ [6] considering an increased traffic distance by $22\,\%$ between 2005 and 2010. For 2002, Burkhardt and Kärcher [10] estimated $RF_{\mathrm{Contrail}} = 0.03\ \mathrm{W\,m^{-2}}$ of contrails and contrail cirrus within a global climate model.

Using satellite data, the Adjusted Forcing AF as imbalance of the Earth-atmosphere energy system after stratospheric temperatures has been adjusted to regain a radiative equilibrium in the stratosphere (assuming zero further radiative heating rates) can be calculated [15, 16], considering a completed transition of contrails into cirrus. Herewith, the diurnal cycle of contrails and cirrus and differences in regions with low and high air traffic demand can be distinguished [16]. Using satellite data of 2006, $AF_{\mathrm{Contrail}} = 0.045$ to $0.075\ \mathrm{W\,m^{-2}}$ has been quantified for contrails and contrail-induced cirrus. A combination of modeled and satellite data-based estimates and a consideration of uncertainties in spreading rate, contrails optical depth, ice particle shape and radiative transfer [17] and accounting for the ongoing increase in air traffic, a contrail and contrail-induced cirrus AF_{Contrail} for the year 2010 of $AF_{\mathrm{Contrail}} = 0.05$ (0.02 to 0.15) $\mathrm{W\,m^{-2}}$ is widely accepted [6].

A consideration of contrails in trajectory optimization tools if any, has been found as constant value for trajectories through ice-supersaturated regions [18–22]. This consequent avoidance of contrail formation does not, however, lead to a holistically optimized trajectory [23]. Specifically, considering single contrails with cooling effects on the Earth-atmosphere system are completely misunderstood in those approaches.

II. Individual Contrails in Trajectory Optimization

The assessment of single contrails in trajectory optimization may be performed in six steps. The procedure is shown in Fig. 1.

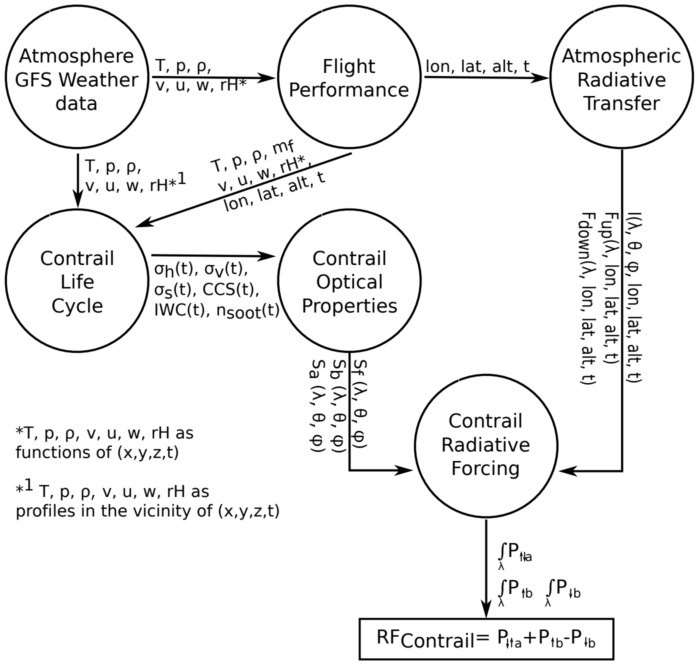

Figure 1. Data flow diagram of all sub models to calculate the radiatitive forcing of individual contrails.

A. Atmosphere GFS Weather Data

First, detailed, weather information of the environment around the aspired route is required. Modeled and gridded global forecast data from the Global Forecast System GFS, provided every six hours in Grib2 format by the National Oceanic and Atmospheric Administration NOAA with a spacial resolution of 0.25 degrees at 18 pressure levels is a good compromise between computational effort and accuracy. For trajectory optimization and the estimation of the conditions of contrail formation, vertical profiles of temperature T [K], pressure p [Pa], density ρ $[\mathrm{kg\,m^{-3}}]$, horizontal wind components u $[\mathrm{m\,s^{-1}}]$ and v $[\mathrm{m\,s^{-1}}]$, vertical velocity w $[\mathrm{Pa\,s^{-1}}]$ and the relative humidity rH [-] along the whole route are taken into account.

B. Flight Performance

Together with typical input variables for trajectory optimization, such as city pair, aircraft type, engine type, payload, optimization function (i.e. minimum fuel burn, minimum time of flight, minimum contrail impact or multi-criteria optimization), a trajectory optimization model with implemented key performance assessment can be used for the calculation of the optimum vertical and lateral path. Here, we use the validated simulation environment TOMATO [24–26] which includes the aircraft performance model COALA [27, 28] for vertical optimization and for the quantification of the emissions. In TOMATO, the trajectory is optimized iteratively by assessing each interim solution regarding several key performance indicators (KPI), contrails amongst others [29]. For comparability, each KPI is transformed into monetary values. For the evaluation of the contrail, the conditions on contrail formation, the fulfilled Schmidt-Appleman-criterion [2, 3] depending on true air speed v_{TAS}, thrust F, fuel flow $\dot{m}_f$ $[\mathrm{kg\,s^{-1}}]$, specific combustion heat of kerosene $Q = 43\ \mathrm{MJ\,kg^{-1}}$, emission index of water vapor $EI_{\mathrm{water}} = 1.24\ \mathrm{kg\,kg^{-1}}$ [11] and the ambient ice supersaturation [30, 31] as function of the relative humidity and the vapor pressure over ice [11] are observed each second.

C. Contrail Life Cycle

In the case both criteria are satisfied, T, p, ρ, u, v, w, rH, longitude lon [°], latitude lat [°], altitude z [m], $\dot{m}_f$ $[\mathrm{kg\,s^{-1}}]$ and time t [s] are provided by COALA for the "Contrail Life Cycle" model [11, 32] of each time step, a contrail is induced. For the initial dimensions, a wake vortex model [33] is applied and calibrated for each aircraft type, implemented in COALA. The initial decay of the contrail in the vortex regime strongly depends on atmospheric turbulence (compare Fig. 2, right), which is approximated by the energy dissipation rate ε $[\mathrm{m^2\,s^{-3}}]$ as conversion of kinetic energy due to molecular friction per unit mass and per time into thermal energy [34]. ε is calculated assuming a lognormal distribution of turbulence in the lower troposphere and upper stratosphere and a linear correlation between a logarithmic diagnostic turbulence value, such as the vertical velocity w, provided by the GFS [35, 36]. Furthermore, wind shear sh $[\mathrm{s^{-1}}]$ (Fig. 2, left) as difference in wind velocity u and v $[\mathrm{m\,s^{-1}}]$ between two altitudes Δz [m] strongly influences the 2D sheared Gaussian plume model for contrail dispersion [11, 32]. Δz is called shear layer and depends on the maximum differences in wind velocity between two altitudes. sh is also calculated from the provided weather data. The sheared diffusivity D_s [$\mathrm{m^2 s^{-1}}$] is assumed to be in the range of the square root of the vertical D_v [$\mathrm{m^2 s^{-1}}$] and horizontal diffusivity D_h [$\mathrm{m^2 s^{-1}}$]: $D_s \approx \sqrt{D_v D_h}$ [37], but $D_s \leq \sqrt{D_v D_h}$ [11]. Assuming a soot emission index of $EI_{\text{soot}} = 0.04\ \mathrm{g\,kg^{-1}}$ kerosene [38] and a proportional share of ice particles in the contrail [38], all variables, impacting the optical properties of the contrail can be provided to the "Contrail Life Cycle" model. In fact, these are the horizontal $\hat{\sigma}_h(t)$ [$\mathrm{m^2}$], vertical $\hat{\sigma}_v(t)$ [$\mathrm{m^2}$] and sheared $\hat{\sigma}_s(t)$ [$\mathrm{m^2}$] components of the contrail diffusivity variance $\hat{\sigma}(t)$ [$\mathrm{m^2}$], the contrail cross section $CCS(t)$ [$\mathrm{m^2}$], the ice water content $IWC(t)$ [$\mathrm{kg\,m^{-3}}$] as total amount of ice mass per volume contrail, the number of ice particles n_p (hereafter called ice particle number density) [$\mathrm{m^-3}$] and the projected particle area A_p [$\mathrm{m^2}$]. The impact of sh, ε and v_z [$\mathrm{m\,s^{-1}}$] on the particle radius and the contrail life time is shown in Fig. 2 and 3, respectively. The vertical wind speed v_z is calculated from the mean divergence of the horizontal wind speed, averaged along the vertical axis between ground and flight level [39]. Thereby, negative values indicate upward wind speeds. On average, values of $\bar{v_z} = -0.005\ \mathrm{ms^{-1}}$ are calculated. The vertical wind velocity is two orders of magnitudes smaller than the horizontal wind velocity and a vertical upwind velocity of $v_z = -0.005\ \mathrm{ms^{-1}}$ is realistic in stable stratification [40]. Assuming this vertical upward speed and a sedimentation of the ice particles following Stoke's law, the contrail sediments as soon as the ice particle radius exceeds values of $r_p \approx 6\ \mu\mathrm{m}$ [11].

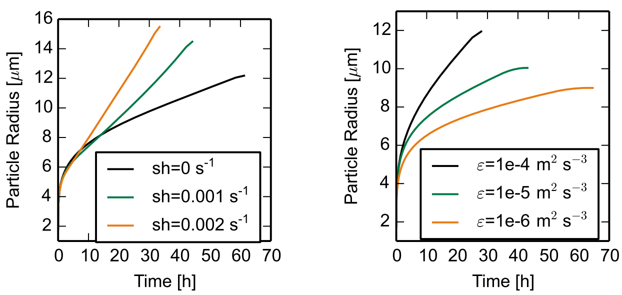

Figure 2. Increasing ice particle radius and decreasing contrail life time with increasing wind shear sh (left) and with decreasing atmospheric turbulence (right).

Note, the available ice water content is distributed equally to the available number of ice particles per contrail volume. A decreasing fuel flow causes less number of soot particles (as primary condensation nuclei), but larger ice particles. However, the optical properties of contrails stronger depend on ice particle size as on ice particle number density [11]. From this follows, that flying slowly through ice-supersaturated regions causes more radiative effective contrails. Furthermore, according to the Schmidt-Appleman-criterion [2, 3], the higher the overall engine efficiency, the lower the exhaust gas temperature, the higher the critical atmospheric temperature (T_{LC}) for contrail formation [41]. In general, optimized air speeds for highly efficient conditions of combustion (i.e. minimum fuel flow) refer to low values of TAS. Both facts support the thesis that cold, ice-supersaturated regions should rather be flown through with high speeds.

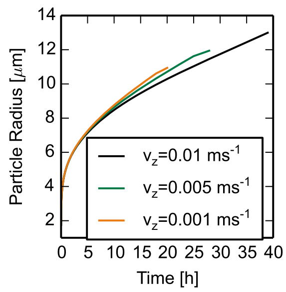

Figure 3. Impact of vertical wind speed v_z on particle radius and contrail life time. The stronger the upward wind, the longer the contrail remains in the ice-supersaturated region.

D. Contrail Optical Properties

The fourth step is the "Contrail Optical Properties" model. Depending on the geometrical and microphysical properties of the contrail, the radiative extinction due to scattering, absorption and emission within the contrail is calculated running a Monte Carlo Simulation to consider multiple scattering events which are likely, especially for large solar zenith angles θ [rad] [11]. Therefore, Beer's law

$$\frac{I_\lambda(s_1)}{I_\lambda(s_2)} = \exp\left[-\int_{s_1}^{s_2} -Q_e\, A_p\, n_p(s)\,\mathrm{d}s\right] \tag{1}$$

is used, where $I_\lambda(s_2)$ and $I_\lambda(s_1)$ denote the original and the extinguished wavelength specific radiation of solar intensities [$\mathrm{W\,m^{-2}sr^{-1}}$] and of terrestrial irradiances [$\mathrm{W\,m^{-2}}$] (compare Fig. 4). $Q_e(s)$ denotes the extinction efficiency [-] and depends on wavelength, particle size and shape [11, 42] and A_p denotes the projected particle area [$\mathrm{m^2}$]. $Q_e(s)$ and A_p(s) are not constant within the contrail and depend on the position s. In the "Contrail Optical Properties" model, $\frac{I_\lambda(s_1)}{I_\lambda(s_2)}$ (1) is interpreted as number ratio of extinguished photons, regardless of the amount of radiation irradiating the contrail (compare Fig. 4) [11, 43].

The extinction of photons is calculated for each direction in space individually, considering ice a particle shape dependent and wavelength dependent probability of an extinguishing event. The latter is described by the absorption and scattering efficiency $Q_a(s)$, $Q_s(s)$. $Q_s(s) + Q_a(s) = Q_e(s)$ are parameterized by Wyser et al. [42] and Yang et al. [44]) as function of wavelength, ice particle size, shape and density, which in turn are provided by the Gaussian plume model (compare Fig. 4).

This "Contrail Optical Properties" model provides weighted number ratios $S_i(\lambda, \mathrm{d}\omega)$ of extinguished photons per meter contrail, per wavelength and per time step of the contrail life cycle (Fig. 4). For each direction of incoming photons, $S_i(\lambda, \mathrm{d}\omega)$ [m] is calculated by

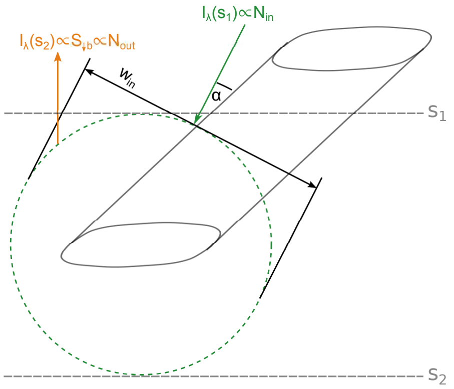

Figure 4. Application of Beer's law to a "Contrail Radiative Forcing" model.

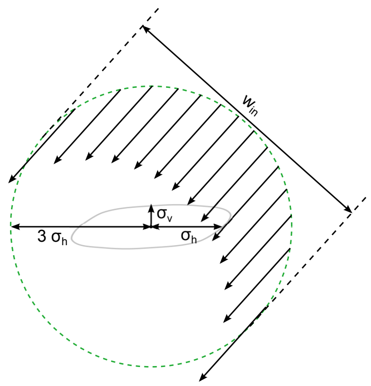

Figure 5. Geometry of the "Contrail Radiative Forcing" model. The contrail is described by a sheared Gaussian plume. The contrail optical properties further depend on the direction of incoming solar intensities and terrestrial irradiances. The circular solution space is defined by the radius $w_{\text{in}} = 6\sigma_h$

$$S_i(\lambda, t, \mathrm{d}\omega) = \frac{N_{\text{out}}}{N_{\text{in}}} w_{\text{in}} \sin\alpha, \tag{2}$$

where N_{out} and $N_{\text{in}} = 10^7$ denote the number on outgoing and incoming photons, respectively. $w_{\text{in}} = 6\hat{\sigma}_h(t)$ denotes the irradiated width of the contrail, α defines the angle between the length axis of the contrail and the incoming photons (compare Fig. 4). This extinction strongly depends on the direction of irradiation (i.e. α). The longer the travel distance of photons through the contrail (i.e. the larger α), the higher the probability that an extinguishing event takes place. With increasing travel distance and with increasing α, the number of outscattered photons increases, although a dominating forward scattering is expected [42, 44, 45]. From this follows, that during horizontal photon transport during sunrise and sunset more photons will be scattered in the opposite hemisphere, compared to a vertical photon transport at noon. However, the contrail radiative extinction further depends on the power with which the contrail is irradiated, which will be maximum at noon and minimum at night. This power is calculated separately in the next step.

E. Atmospheric Radiative Transfer

The fifth step of the approach provides wavelength and angular specific solar intensities and terrestrial irradiances, at the position of the contrail. This step is necessary, because the radiative extinction due to the contrail does not only depend on the optical properties of the contrail itself, but also on the amount of radiation, irradiating the contrail. The powers of solar intensities and terrestrial irradiances depend on wavelength, longitude, latitude, altitude, the presence of clouds, time of the day and time of the year. Most of these input variables are provided by the flight performance model (compare Fig. 1). For the calculation of this "Atmospheric Radiative Transfer", the radiative transfer software package libRadtran [46] is used. Due to different properties of solar and terrestrial extinction in the atmosphere, different radiative transfer solvers are used.

1) Terrestrial Radiative Transfer: In the terrestrial wavelength spectrum ($3 \leq \lambda \leq 100\ \mu$m), absorption by atmospheric molecules strongly depends on wavelength and varies between neighboring wavelengths. These narrow absorption bands require a high spectral resolution in the radiative transfer calculation and therefore a high computational effort. However, a weak angular dependence (described by zenith angle θ and azimuthal angle ϕ) of radiation due to a missing part of direct irradiance is expected. The Two Stream Approximation (TSA) takes advantage of the weak angular dependence and reduces the computational effort [47]. Here, all shares of radiation coming from one hemisphere are azimuthally averaged over the half space and are treated as a single irradiance F [$\mathrm{W\,m^{-2}}$] without specific information about the angular direction (compare Fig. 6, left). Due to this average, two irradiances at any altitude remain: terrestrial irradiances coming from the lower hemisphere

$$F_{\text{up}}(\lambda, t, \theta = {}^1\!/_2\pi ... {}^3\!/_2\pi) \tag{3}$$

and terrestrial irradiances coming from the upper hemisphere

$$F_{\text{down}}(\lambda, t, \theta = {}^3\!/_2\pi ... {}^1\!/_2\pi) \tag{4}$$

(compare Fig. 6, left) [11].

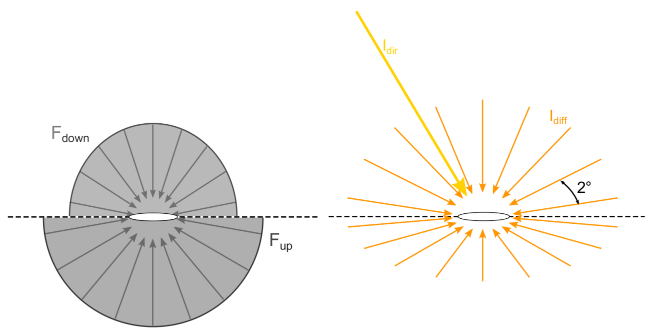

Figure 6. Azimuthally averaged terrestrial irradiances F_{up} and F_{down} (left) and angular dependent diffuse solar intensities $I_{\text{diff}}(\theta, \phi)$. The direct beam I_{dir} coming from the sun is added to the corresponding solid angle of the position of the sun.

2) Solar Radiative Transfer: In the solar wavelength spectrum ($0 \leq \lambda \leq 4$ μm, compare Fig. 7) a TSA is out of question, because of a large influence of the direct beam (in the direction of the position of the sun) on the radiation field. This influence causes a strong angular radiative dependence which cannot be described by a TSA. The radiative transfer solver DISORT (DIScrete Ordinate Radiative Transfer solver) is used for the angular dependent calculation of direct (5) solar intensities (5) [$\mathrm{mW\,sr^{-1}m^{-2}nm^{-1}}$] calculated.

$$I_{\mathrm{dir}}(\lambda, t, \mathrm{lon}, \mathrm{lat}, \Omega) \tag{5}$$

Here, the direction of the direct beam, Ω [sr], is described by the solar zenith angle and the solar azimuthal angle. Diffuse solar intensities (6) [$\mathrm{mW\,sr^{-1}m^{-2}nm^{-1}}$]

$$I_{\mathrm{diff}}(\lambda, t, \mathrm{lon}, \mathrm{lat}, \theta, \phi) \tag{6}$$

depending on longitude, latitude, altitude, time of the day and time of the year [48] are also provided by DISORT. DISORT is the most used, recommended and most updated solver for angular depending radiative transfer in the shortwave spectrum [11, 49]. Diffuse solar intensities I_{diff} are calculated with an angular discretization of $\mathrm{d}\theta = \mathrm{d}\phi = 2°$ and the direct beam I_{dir} is added to the solid angle $\mathrm{d}\omega$ [sr]

$$\mathrm{d}\omega = \sin\theta\,\mathrm{d}\theta\,\mathrm{d}\phi, \tag{7}$$

where θ and ϕ, are the solar zenith and azimuthal angle, respectively (compare Fig. 6, right) [11]. Fig. 7 clearly indicates the different contributions of wavelength-specific irradiances on the radiation budget of the Earth-Atmosphere System. Hence, a consideration of solar irradiances around the maximum at $\lambda = 0.55$ (i.e. $0.2 < \lambda < 1$ μm) would be sufficient. Terrestrial irradiances should be considered between $5 < \lambda < 22$ μm. Additionally, Fig. 7 proves the significant impact of atmospheric absorption by comparing the modeled irradiances with the theoretical values, calculated with Planck's function assuming mean temperatures of 5750 K of the sun and 288 K of the Earth's surface.

F. Contrail Radiative Forcing

The radiative quantities of the "Atmospheric Radiative Transfer" model are multiplied with the extinguished number ratios, provided by the "Contrail Optical Properties" model to estimate the wavelength specific and direction specific extinction of radiation due to the contrail. Because the contrail radiative forcing is defined as imbalance of the radiation budget at a horizontal layer, we distinguish between sources and drains of radiation in the upper and in the lower hemisphere of the contrail (compare Fig. 8).

To calculate the radiative forcing per unit length of the contrail, the power $P_i(\lambda, t, \mathrm{lon}, \mathrm{lat}, \mathrm{d}\omega)$ [$\mathrm{W\,m^{-1}\,nm^{-1}}$] of the extinguished photons once irradiated on a unit length contrail have to be considered and balanced. Therefore, the solar intensities (6) and the terrestrial irradiances (3) and (4) coming from a particular solid angle $\mathrm{d}\omega$ [sr], (calculated

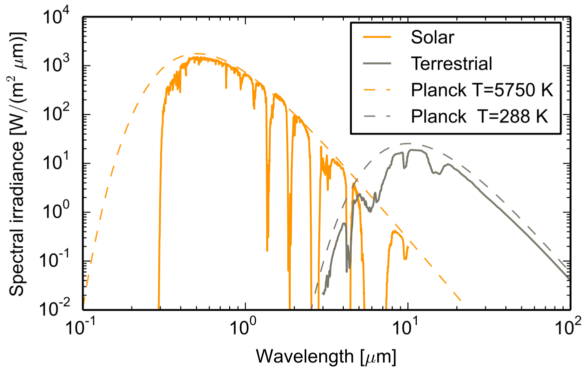

Figure 7. Modeled and approximated (as Planck's function) solar and terrestrial irradiances over Berlin, Germany in 10000 m altitude. The extinction of radiation by the atmosphere (without contrail) is remarkable for solar wavelengths < 0.2 μm and for the whole terrestrial wavelength spectrum.

by the "Atmospheric Radiative Transfer" model) has to be weighted by the weighted number ratios of extinguished photons S_i [m] (2) (from the "Contrail Optical Properties" model) and the corresponding solid angle $\mathrm{d}\omega_i$. Therefore, only the backscattered and absorbed powers are of interest and the extinguished powers can be summarized to the following components (compare Fig. 8):

- $P_{\uparrow\downarrow a}$: number of absorbed photons coming from below
- $P_{\uparrow b}$: number of photons coming from below, scattered into the lower hemisphere
- $P_{\downarrow b}$: number of photons coming from above, scattered into the upper hemisphere

For radiation coming from a particulate solid angle $\mathrm{d}\omega_i$ (7) and getting scattered into the same hemisphere (i.e. backscattered) the extinguished power $P_b(\lambda, t, \mathrm{lon}, \mathrm{lat}, \mathrm{d}\omega_i)$ [$\mathrm{W\,m^{-1}nm^{-1}}$] is

$$\begin{aligned}
P_{\downarrow b}(\lambda, t, \mathrm{d}\omega_i) &= I(\lambda, t, \mathrm{d}\omega_i) \cdot S_b(\lambda, t, \mathrm{d}\omega_i) \cdot \mathrm{d}\omega_i \\
P_{\uparrow b}(\lambda, t, \mathrm{d}\omega_i) &= I(\lambda, t, \mathrm{d}\omega_i) \cdot S_b(\lambda, t, \mathrm{d}\omega_i) \cdot \mathrm{d}\omega_i \\
P_{\downarrow\uparrow a}(\lambda, t, \mathrm{d}\omega_i) &= I(\lambda, t, \mathrm{d}\omega_i) \cdot S_a(\lambda, t, \mathrm{d}\omega_i) \cdot \mathrm{d}\omega_i,
\end{aligned}$$

where $S_b(\lambda, t, \mathrm{d}\omega_i)$ denotes the weighted number ratio of backscattered photons coming from a particular solid angle $\mathrm{d}\omega_i$ and getting scattered into the same hemisphere and $I(\lambda, t, \mathrm{d}\omega_i)$ is the wavelength specific solar intensity from the particular solid angle $\mathrm{d}\omega_i$. In the same way, absorbed solar powers $P_{\downarrow\uparrow a}(\lambda, t, \mathrm{lon}, \mathrm{lat}, \mathrm{d}\omega_i)$ are calculated for each wavelength λ and each solid angle $\mathrm{d}\omega_i$.

Terrestrial irradiances F_{up} and F_{down} [$\mathrm{W\,m^{-2}nm^{-1}}$], calculated with the Two Stream Approximation are hemispherically averaged irradiances. To estimate the extinguished power in the terrestrial wavelength spectrum, F_{up} and F_{down} have to weighted by the number ratio of extinguished photons coming from the upper hemisphere $S_{\downarrow b}$ and the lower hemisphere $S_{\uparrow b}$ both getting scattered into the same hemisphere as they are coming from and the absorbed photons coming from all directions $S_{\downarrow\uparrow a}$. For example:

$$P_{\downarrow b}(\lambda, t) = F_{\text{down}}\, S_{\downarrow b}(\lambda, t) \tag{8}$$
$$P_{\uparrow b}(\lambda, t) = F_{\text{up}}\, S_{\uparrow b}(\lambda, t) \tag{9}$$
$$P_{\downarrow\uparrow a}(\lambda, t) = F_{\text{down}}(\lambda, t)\, S_{\downarrow a}(\lambda, t) \tag{10}$$
$$+\, F_{\text{up}}(\lambda, t)\, S_{\uparrow a}(\lambda, t). \tag{11}$$

The backscattered powers $P_{b,}(\lambda, t, \text{lon}, \text{lat}, \text{d}\omega)$ are categorized into two classes: first, backscattered powers from the upper hemisphere $P_{\downarrow b}(\theta = \frac{3}{2}\pi ... \frac{1}{2}\pi)$ (resulting in a cooling effect) and second from the lower hemisphere $P_{\uparrow b}(\theta = \frac{1}{2}\pi ... \frac{3}{2}\pi)$ (with a heating effect, compare Fig. 8). Absorbed powers $P_{\downarrow\uparrow a}(\lambda, t, \text{lon}, \text{lat}, \text{d}\omega)$ coming from both hemispheres always contribute to a contrail heating. Those components contribute to the radiative forcing RF_{Contrail}

$$RF_{\text{Contrail,m}} = P_{\downarrow\uparrow a} + P_{\uparrow b} - P_{\downarrow b}. \tag{12}$$

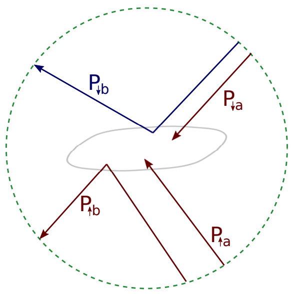

Figure 8. Components of backscattered and absorbed powers contributing to the contrail radiative forcing (compare (12)). Blue parts denote cooling effects, red parts indicate warming effects.

After integrating over all significant wavelengths, time steps of the contrail life cycle and over the contrail length, each with different optical properties $S_i(\lambda, t)$, the total radiative forcing $RF_{\text{Contrail,m}}$ [$\text{W}\,\text{m}^{-1}$] (12) per meter of an individual contrail can be estimated. By multiplying (12) with the length L_{Contrail} of the contrail with similar optical properties offers the extinguished power [W] due the contrail. Usually, the radiative forcing is related to the Earth's surface, which is $A_{\text{Earth}} = 5.1 \cdot 10^{14}\ \text{m}^2$. Hence, the estimated extinguished power is divided by A_{Earth}.

$$RF_{\text{Contrail}} = \frac{RF_{\text{Contrail,m}}\ L_{\text{Contrail}}}{A_{\text{Earth}}}. \tag{13}$$

G. Weighting of Contrail Costs in Trajectory Optimization

The integration of RF_{Contrail} over the whole life cycle, over all significant wavelengths and the division by A_{Earth} offers a comparison with the impact of a reference emission (e.g. CO_2) over the whole flight.

Usually, a certain time horizon H (e.g. $H = 100$ years) is considered in those interpretations. In this case, the ratio of RF_{Contrail} over RF_{CO_2} (known as the global warming potential GWP)

$$GWP = \frac{\int_0^H RF_{\text{Contrail}}(t)\text{d}t}{\int_0^H RF_{CO_2}(t)\text{d}t} \tag{14}$$

is used to calculate CO_2 equivalent emissions, which are transferred into monetary values by applying political instruments, such as the emission trading scheme ETS. For instance, for $H = 100$ years, the radiative forcing of the total amount of CO_2 in the atmosphere is [50]

$$\int_0^{H=100} RF_{CO_2}(t)\text{d}t = \alpha_{CO_2} \ln\left(\frac{\text{C}}{\text{C}_0}\right) = 1.94\ \text{W}\,\text{m}^{-2} \tag{15}$$

where $\alpha_{CO_2} = 5.35$ denotes a constant [50], $\text{C} = 399.39$ ppm is the actual concentration of CO_2 [51] and $\text{C}_0 = 278$ ppm is the pre-industrial concentration of CO_2 in 1959 [51].

Equation (15) considers the total sum of CO_2 emissions in 100 years and is not restricted to the aviation transport sector. The radiative impact of CO_2 strongly depends on the altitude of emission. In high altitudes (above the tropopause with low vertical exchange) CO_2 exists for 400 years. In low altitudes (below the tropopause) precipitation induces washing-off effects of CO_2. Those large differences in the residence time, complicate the use of (15) for a comparison of aviation induced radiative forcing due to contrails and CO_2 emissions.

However, from the literature review in the introduction of this paper we know the amount of CO_2 emissions, caused by aviation in 2005

$$m_{CO_2,2005} = 733\ 10^6\ \text{t}\,\text{a}^{-1} \tag{16}$$

[7] and the radiative forcing of those emissions

$$RF_{CO_2,2005} = 0.028\ \text{W}\,\text{m}^{-2}. \tag{17}$$

Hence, the impact of each tonne CO_2 emitted by aviation in 2005 was

$$RF_{CO_2} = 3.8\ 10^{-11}\ \text{W}\,\text{m}^{-2}\text{t}_{CO_2}^{-1}. \tag{18}$$

Therewith, the radiative forcing of an individual contrail (13) can be transformed into tonnes of CO_2 equivalent emissions, which can be used as external costs in a multi-criteria trajectory optimization.

$$m_{CO_2\text{eq}} = \frac{RF_{\text{Contrail}}}{3.8\ 10^{-11}\ \text{W}\,\text{m}^{-2}\text{t}_{CO_2}^{-1}}. \tag{19}$$

By weighting the price per tonne of CO_2 equivalent emission, contrails are considered in the multi-criteria trajectory optimization TOMATO. Following global approximations, as elaborated in the introduction, it is expected, that the radiative impact of a single flight's contrail exceeds those effects of CO_2.

III. Results

The most important effects of RF_{Contrail} are determined by the angle α between the length axis of the contrail and the incoming photons (compare Fig. 4), because it determines the travel distance of photons through the contrail. Furthermore, RF_{Contrail} depends on the order of magnitude of incoming radiation, depending on wavelength (solar $>$ terrestrial), time of the day and year (summer, noon $>$ winter, morning and evening) and on latitude (equator $>$ pole). Both effects are shown in Fig. 9, because α and solar intensity change with daytime. Although the amount of backscattered power $P_{\downarrow b}$ dominates over the whole day, the sum of downward backscattered power $P_{\uparrow b}$ and absorbed power $P_{\downarrow\uparrow a}$ nearly compensates $P_{\downarrow b}$ between 7 a.m. and 5 p.m. Only during sunrise and sunset with horizontal photon transport (around 6 a.m. and 6 p.m.), RF_{Contrail} is significantly negative. For astrologic reasons, the "sunrise-sunset effect" increases with increasing latitude, but the amplitude in Fig. 9 decreases with increasing latitude.

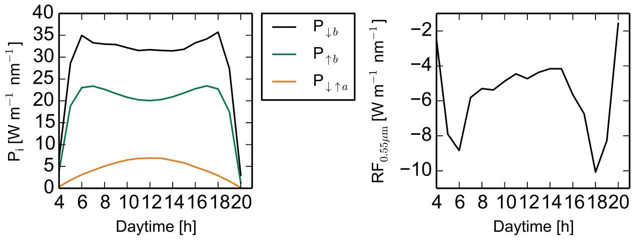

Figure 9. Left: Backscattered power for diurnal variations of upward ($P_{\uparrow b}$) and downward ($P_{\downarrow b}$) solar radiation ($\lambda = 0.55$ μm) and absorbed power of downward and upward radiation ($P_{\downarrow\uparrow a}$) for a contrail in June over Berlin, Germany, which constitutes the North-South axis. Right: resulting RF_{Contrail} (12) from the components shown left.

Although in Fig. 9 the extinguished of only a single wavelength is shown, the results my be transferred to the narrow wavelength band around $0.2 < \lambda < 2$ μm. In Fig. 10, simulations of the whole solar spectrum with significant contribution to the energy budget with wavelengths between 0.55 μm $\leq \lambda \leq 4.5$ μm (left) and of the most important terrestrial spectrum wavelengths between 4.5 μm $\leq \lambda \leq 21.5$ μm (right) are shown. Fig. 10, left, indicates a decreasing solar effect with increasing wavelength due to a decreasing solar intensity and due to an increasing share of absorbed power. However, with increasing wavelength, positive values of RF_{contrail} become more dominant. Note, in Fig. 9 and 10 only the radiative properties of a single contrail with specific optical properties are calculated. The absorption efficiency Q_a, known as the possibility of an absorbing event within the contrail strongly varies with ice particle size and shape, which is why the fluctuation in Fig. 10 (left) is very contrail-specific.

The strong impact of ice particle size on Q_a causes an increasing terrestrial radiative forcing with increasing contrail lifetime (compare Fig. 11 and Fig. 2 and 3 for increasing ice particle radius with lifetime). Additionally, an increasing contrail width with life time causes a more distinct radiative forcing of older contrails. Note, the solar radiative forcing (Fig. 11, left) is shown, only for a single wavelength $\lambda = 0.55$ μm, whereas the terrestrial RF_{Contrail} is integrated over the whole significant terrestrial spectrum 4.5 μm $\leq \lambda \leq 21.5$ μm. The large computational effort requires the reduction of the number of calculations, especially in the solar wavelength spectrum.

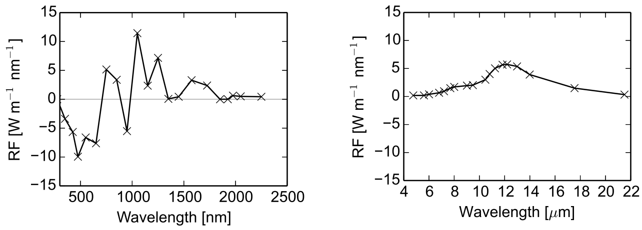

Figure 10. Wavelength dependent contrail radiative forcing of a single contrail over Berlin, Germany. In Mid-latitudes, the impact of solar extinction is more significant than the terrestrial contribution to RF_{Contrail}. With increasing wavelength RF_{Contrail} converges to a balanced positive value.

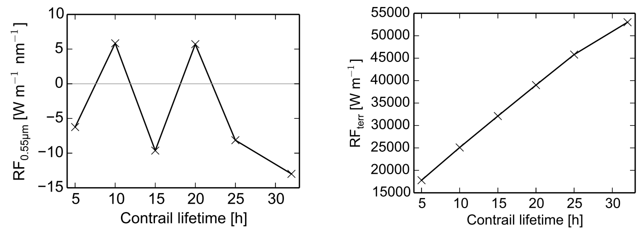

Figure 11. Solar RF_{Contrail} at $\lambda = 0.55$ μm depending on the life cycle of single contrail (left). Right: increasing terrestrial RF_{Contrail} with contrail life time, integrated over the whole significant terrestrial spectrum 4.5 μm $\leq \lambda \leq 21.5$ μm.

Finally, the impact of the consideration of contrails in trajectory optimization is exemplified in Fig. 12. Here, blue squares denote ice-supersaturated regions wherein contrail formation is very likely. For this example flight from Los Angeles (LAX) to Boston (BOS) different routes are calculated and compared with each other. The originally filed route (black, 4580 km ground distance) induced a contrail with a length of $L_{\text{Contrail}} = 1705$ km ground distance. The mean optical properties of this contrail have been estimated to $RF_{\text{Contrail}} = 0.305$ W m^{-1} which is 3.1 10^{-6}W m^{-2}. Following (19), this contrail must be weighted with 81578 t CO_2 equivalent emissions. Considering this weighting in a multi-criteria trajectory optimization, the contrail would have been completely avoided (red route in Fig. 12 with 4730 km ground distance). A more harmonized trajectory with a reduced contrail length of $L_{\text{Contrail}} = 1374$ km ground distance constitutes the green route in Fig. 12 with a total ground distance of 4246 km and a contrail weighting of 66087 t CO_2 equivalent emissions.

IV. Conclusions

In this study, a method is described to consider the environmental impact of individual condensation trails in a multi-criteria trajectory optimization. A tendency towards lower

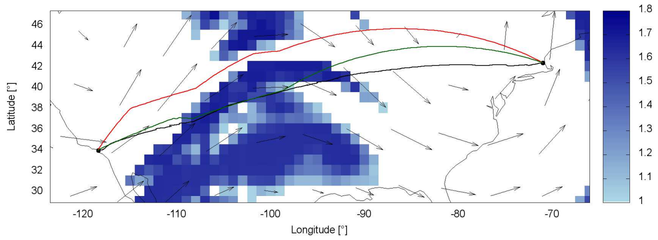

Figure 12. Lateral routes of optimized trajectories between Los Angeles and Boston with different contrail weightings in an ice-supersaturated atmosphere (blue squares). Significant differences between the filed route (black), a weighting of 32 tonnes CO_2 (green) and a weighting of 40 tonnes CO_2 (red) per hour contrail formation leads to a complete contrail avoidance.

aircraft speeds and higher fuel flows has been identified to decrease the probability of contrail formation. The atmospheric parameters wind shear, vertical wind speed and turbulence mainly influence the initial contrail dimensions (weak turbulence: small contrail) and the contrail life time (strong turbulence: short life time). To consider multiple scattering events a Monte Carlo Simulation is neccessary, where the position and the kind of extinction event are determined probabilistically. The radiative extinction due to the contrail is calculated separately from the atmospheric radiative extinction. The advantage of this approach is, that radiative properties of optically similar contrails (calculated in the "Contrail Optical Properties" model) can be easily combined with different atmospheric conditions (estimated in the "Atmospheric Radiative Transfer" model), which are a function of the position, time of the day and year. In Mid-Latitudes, even during daytime the warming effect of the contrail dominates, mainly because of an increasing absorbed power with increasing contrail life time in the terrestrial wavelength spectrum. A significant impact of the track angle (i.e. the contrail length axis) on the radiative properties has been elaborated because it determines the travel distance of photons during sunrise and sunset. However, suggestions of preferring North-South oriented routes to East-West routes is less helpful in daily operations.

Acknowledgment

This work is financed by the Federal Ministry for Economic Affairs and Energy in the framework of the research project ProfiFuel.

References

[1] U. Schumann, "Formation, properties and climatic effects of contrails," *C.R. Physique*, vol. 6, pp. 549–565, 2005.
[2] E. Schmidt, "Die Entstehung von Eisnebel aus den Auspuffgasen von Flugmotoren," *Schriften der Deutschen Akademie der Luftfahrtforschung, Verlag R. Oldenbourg, München/Berlin*, vol. 44, pp. 1–15, 1941.
[3] H. Appleman, "The formation of exhaust condensation trails by jet aircraft," *Bulletin of the American Meteorological Society*, vol. 34, pp. 14–20, 1953.
[4] W. (WMO). Cloud atlas. [Online]. Available: https://cloudatlas.wmo.int/aircraft-condensation-trails.html
[5] R. Meerkötter, U. Schumann, P. Minnis, D. R. Doelling, T. Nakajima, and Y. Tsushima, "Radiative forcing by contrails," *Journal of Geophysical Research*, vol. 17, pp. 1080–1094, 1999.
[6] G. Myhre, D. Shindell, F.-M. Bréon, W. Collins, J. Fuglestvedt, J. Huang, D. Koch, J.-F. Lamarque, D. Lee, B. Mendoza, T. Nakajima, A. Robock, G. Stephens, T. Takemura, and H. Zhang, "Anthropogenic and natural radiative forcing. in: Climate change 2013: The physical science basis. contribution of working group i to the fifth assessment report of the intergovernmental panel on climate change," *Cambridge University Press*, 2013.
[7] D. S. Lee, D. W. Fahey, P. M. Forster, P. J. Newton, R. C. Witt, L. L. Lim, B. Owen, and R. Sausen, "Aviation and global climate change in the 21st century," *Atmospheric Environment*, vol. 43, pp. 3520–3537, 2009.
[8] P. Minnis, U. Schumann, D. R. Doelling, K. M. Gierens, and D. W. Fahey, "Global distribution of contrail radiative forcing," *Geophysical Research Letters*, vol. 26, pp. 1853–1856, 1999.
[9] R. Sausen, I. Isaksen, V. Grewe, D. Hauglustaine, D. S. Lee, G. Myhre, M. Köhler, G. Pitari, U. Schumann, F. Stordal, and C. Zerefos, "Aviation radiative forcing in 2000: An update on ipcc (1999)," *Meteorologische Zeitschrift*, vol. 14, pp. 555–561, 2005.
[10] U. Burkhardt and B. Kärcher, "Global radiative forcing from contrail cirrus," *Nature Climate Change*, vol. 1, pp. 54–58, 2011.
[11] J. Rosenow, "Optical properties of condenstation trails," Ph.D. dissertation, Technische Universität Dresden, 2016.
[12] P. Spichtinger, "Eisübersättigte Regionen," Ph.D. dissertation, University of Munich, Department of Physics, Mai 2004. [Online]. Available: http://nbn-resolving.de/urn:nbn:de:bvb:19-28643
[13] A. Gounou and R. J. Hogan, "A sensitivity study of the effect of horizontal photon transport on the radiative forcing of contrails," *Journal of Atmospheric Sciences*, vol. 64, pp. 1706–1716, 2007.
[14] L. Forster, C. Emde, B. Mayer, and S. Unterstrasser, "Effects of three-dimensional photon transport on the radiative forcing of realistic contrails," *American Meteorological Society*, pp. 2243–2255, 2011.
[15] K. Shine, J. Cook, E. J. Highwood, and M. M. Joshi, "An alternative to radiative forcing for estimating the relative importance of climate change mechanisms," *Geophysical Research Letters*, vol. 30, no. 20, 2003.
[16] U. Schumann and K. Graf, "Aviation-induced cirrus and radiation changes at diurnal timescales," *Journal of Geophysical Research*, vol. 118, pp. 1–18, 2013.
[17] K. M. Markowicz and M. L. Witek, "Simulations of contrail optical properties and radiative forcing for various crystal shapes," *Journal of Applied Meteorology and Climatology*, vol. 50, 2011.
[18] B. Sridhar and N. Y. Chen, "Fuel efficient strategies for reducing contrail formations in united states airspace," in *Proceeding of the 29th IEEE/AIAA Digital Avionics Systems Conference (DASC)*, I. of Electrical & ElectronicsEngineers (IEEE), Ed., 2010.
[19] B. Sridhar, N. Y. Chen, and H. K. Ng, "Energy efficient contrail mitigation strategies for reducing the environmental impact of aviation," in *10th USA/Europe Air Traffic Management R&D Seminar Chicago*, 2013.
[20] V. Grewe, S. Matthes, K. Dahlmann, V. Gollnick, M. Niklaß, F. Linke, and K. Kindler, "Climate impact evaluation of future green aircraft technologies," in *Greener Aviation, Brussels*, 2016.
[21] S. Matthes, V. Grewe, D. Lee, F. Linke, K. Shine, and S. Stromatas, "Atm4e: A concept for environmentally-optimized aircraft trajectories," in *Greener Aviation, Brussels*, 2016.
[22] J. Rosenow, S. Förster, M. Lindner, and H. Fricke, "Impact of multi-criteria optimized trajectories on european air traffic density, efficiency and the environment," in *Twelfth USA/Europe Air Traffic Management Research and Development Seminar (ATM2017)*, 2017.
[23] J. Rosenow and M. Schultz, "Coupling of turnaround and trajectory optimization in an air traffic simulation," in *Winter Simulation Conference*, 2018.
[24] S. Förster, J. Rosenow, M. Lindner, and H. Fricke, "A toolchain for optimizing trajectories under real weather conditions and realistic flight performance," in *Greener Aviation, Brussels*, 2016.
[25] J. Rosenow, H. Fricke, and M. Schultz, "Air traffic simulation with 4d multi-criteria optimized trajectories," in *Proceedings of the 2017 Winter Simulation Conference*, W. K. V. C. et al., Ed., 2017.
[26] J. Rosenow, S. Förster, M. Lindner, and H. Fricke, "Multicriteria-optimized trajectories impacting today's air traffic density, efficiency, and environmental compatibility," *Journal of Air Transportation*, 2018.
[27] J. Rosenow and H. Fricke, "Flight performance modeling to optimize trajectories," in *Deutscher Luft- und Raumfahrtkongress 2016*, 2016.
[28] J. Rosenow, S. Förster, and H. Fricke, "Continuous climb operations with minimum fuel burn," in *Sixth SESAR Innovation days*, 2016.

[29] J. Rosenow, S. Förster, M. Lindner, and H. Fricke, “Multi-objective trajectory optimization,” *International Transportation*, vol. Special Edition 1, 2016.

[30] R. Sussmann and K. M. Gierens, “Lidar and numerical studies on the different evolution of vortex pair and secondary wake in young contrails,” *J. Geophys. Res.*, vol. 104, pp. 2131–2142, 1999.

[31] ——, “Differences in early contrail evolution of two-engine versus four-engine aircraft: Lidar measurements and numerical simulations,” *Journal of Geophysical Research*, vol. 106, pp. 4899–4911, 2001.

[32] J. Rosenow, M. Kaiser, and H. Fricke, “Modeling contrail life cycles based on highly precise flight profile data of modern aircraft,” in *Proceedings of the International Conference on Research in Airport Transportation (ICRAT)*, 2012.

[33] F. Holzäpfel, “Probabilistic two-phase wake vortex decay and transport model,” *Journal of Aircraft*, vol. 40, no. 323-331, 2003.

[34] T. Foken, *Angewandte Meteorologie*. Springer-Verlag Berlin Heidelberg, 2006.

[35] R. D. Sharman, L. B. Cornman, G. Meymaris, and J. Pearson, “Description and derived climatologies of automated in situ eddy-dissipation-rate reports of atmospheric turbulence,” *Journal of Applied Meteorology and Climatology*, vol. 53, 2014.

[36] R. D. Sharman and J. M. Pearson, “Prediction of energy dissipation rates for aviation turbulence. part i: Forecasting nonconvective turbulence,” *Journal of Applied Meteorology and Climatology*, vol. 56, 2017.

[37] U. Schumann, P. Konopka, R. Baumann, R. Busen, T. Gerz, D. Schlager, P. Schulte, and H. Volkert, “Estimate of diffusion parameters of aircraft exhaust plumes near the tropopause from nitric oxide and turbulence measurements,” *Journal of Geophysical Research*, vol. 100, pp. 14 147–14 162, 1995.

[38] A. Döplheuer and M. Lecht, “Influence of engine performance on emission characteristic,” *RTO MP-14. Lisabon, Portugal*, 1998.

[39] H. Kraus, *Die Atmosphäre der Erde*. Springer-Verlag Berlin Heidelberg, 2001.

[40] W. Roedel, *Physik unserer Umwelt, die Atmosphäre*. Springer-Verlag Berlin Heidelberg, 2000.

[41] U. Schumann, “On conditions for contrail formation from aircraft exhaust,” *Meteorologische Zeitschrift*, vol. 5, pp. 4–23, 1996.

[42] P. Yang, K. N. Liou, K. Wyser, and D. Mitchell, “Parameterization of the scattering and absorption properties of individual ice crystals,” *Journal of Geophysical Research*, vol. 105, pp. 4699–4718, 2000.

[43] A. Einstein, “Über einen die erzeugung und verwandlung des lichtes betreffenden heuristischen gesichtspunkt,” *Annalen der Physik*, vol. 17, pp. 132–148, 1905.

[44] P. Yang, H. Wei, H.-L. Huang, B. A. Baum, Y. X. Hu, G. W. Kattawar, M. I. Mishchenko, and Q. Fu, “Scattering and absorption property database for nonspherical ice particles in the near- through far-infrared spectral region,” *Applied Optics*, vol. 44, pp. 5512–5523, 2005.

[45] A. Macke, P. N. Francis, G. M. McFarquhar, and S. Kinne, “The role of ice particle shapes and size distributions in the single scattering properties of cirrus clouds,” *American Meteorological Society*, 2010.

[46] B. Mayer and A. Kylling, “Technical note: The libradtran software package for radiative transfer calculations description and examples of use,” *Atmospheric Chemistry and Physics*, vol. 5, pp. 1855–1877, 2005.

[47] A. Kylling, K. Stamnes, and S.-C. Tsay, “A reliable and efficient two-stream algorithm for spherical radiative transfer: Documentation of accuracy in realistic layered media,” *Journal of Atmospheric Chemistry*, vol. 21, no. 115-150, 1995.

[48] K. Stamnes, S.-C. Tsay, W. Wiscombe, and K. Jayaweera, “Numerically stable algorithm for discrete-ordinate-method radiative transfer in multiple scattering and emitting layered media,” *Applied Optics*, vol. 27, pp. 2502–2509, 1988.

[49] B. Mayer, A. Kylling, C. Emde, U. Hamann, and R. Buras, “libradtran user's guide,” Technische Universität München, Tech. Rep., 2011.

[50] P. Forster, V. Ramaswamy, P. Artaxo, T. Berntsen, R. Betts, D. Faheya, J. Haywood, J. Lean, D. Lowe, G. Myhre, J. Nganga, R. Prinn, G. Raga, M. Schulz, and R. V. Dorland, *Changes in Atmospheric Constituents and in Radiative Forcing, in: Climate Change 2007: The Physical Science Basis. Contribution of Working Group I to the Fourth Assessment Reportof the Intergovernmental Panel on Climate Change*. Cambridge University Press, 2007.

[51] E. D. und P. Tans, “National oceanic and atmospheric administration earth system research laboratory website,” 2019. [Online]. Available: www.esrl.noaa.gov/gmd/ccgg/trends/

AUTHOR BIOGRAPHY

Judith Rosenow (born in Berlin, Germany in 1983) studied Hydrology at Technische Universität Dresden from 2003 to 2008 where she specialized in Meteorology during her diploma thesis. In 2016 she finished her PhD at Technische Universität Dresden with focus on optical properties of condensation trails aiming the possibility of optimizing a flight trajectory with respect to minimum climate impact of the generated contrail. Since 2014 she is project leader of the projects MEFUL and ProfiFuel at Technische Universität Dresden.

Hartmut Fricke (born in Berlin, Germany in 1967) studied Aeronautics and Astronautics at Technische Universität (TU) Berlin from 1985-1991 where he also received his doctor in ATM. In 2001 he finished his Habilitation on “Integrated Collision Risk Modeling for airborne and ground based systems”. Since December 2001, he is professor for Aviation Technologies and Logistics at TU Dresden. In 2006 he was appointed Member of the Scientific Advisory Board to the German Federal Minister of Transport. He is member of various journal review committees. In 2012 he was elected scientific expert to DFG. In 2013 he became SESAR External Expert.